Ultimate behaviour of hybrid stainless steel cross-sections

Marina Bock [a], Michaela Gkantou [b], Marios Theofanous [c], Sheida Afshan [d], Huanxin Yuan [e]

[a] School of Architecture and Built Environment, University of Wolverhampton, UK
[b] School of Civil Engineering and Built Environment, Liverpool John Moores University, UK
[c] Department of Civil Engineering, University of Birmingham, Birmingham, UK
[d] University of Southampton, Department of Civil, Maritime and Environmental Engineering UK
[e] School of Civil Engineering, Wuhan University, Wuhan, PR China

Abstract

Hybrid steel plate girders are used worldwide as primary structural members in steel and composite bridges, when there is a need for deeper sections with greater stiffness and bending resistance than rolled sections to carry heavy loads. With the increasing importance of sustainability and lifecycle (cost) analysis, design for maintenance has become an important consideration for infrastructure projects like bridges which have a design working life exceeding 100 years over which they need to be regularly inspected and maintained. Stainless steels are known for their excellent corrosion resistance and low maintenance costs and thus the application of hybrid plate girders in bridge designs could be explored. This paper reports a numerical study on stainless steel hybrid plate girders subjected to compression and to bending and assesses relevant recommendations for their design. Previously developed FE models validated against stub column and four-point bending tests are employed and a parametric study is conducted on hybrid I-sections over a wide range of cross-section slenderness and aspect ratios. Based on the obtained results, the EN 1993-1-4 design predictions for stainless steel cross-sections in compression and in bending are assessed and the accuracy of the codified slenderness limits for both homogeneous and hybrid stainless steel girders is discussed. Furthermore, the numerically obtained deformation capacity at ultimate load is plotted against the CSM base curve originally derived for homogeneous sections and the accuracy of the CSM predictions of the cross-section resistance is also assessed, demonstrating that the CSM can be employed to predict the cross-section resistance of hybrid girders.

1. Introduction

Medium and long-span steel and composite bridges often employ plate girders as primary structural members due to the inadequacy of rolled sections to safely carry the design loads [1]. A plate girder may be designed as homogenous or as hybrid when financial considerations dictate the use of the more expensive higher strength material in the flanges with the web employing a more economical lower grade material. Hybrid I-sections are known to be more efficient, compared to equivalent homogeneous sections, in terms of strength, which may lead to serviceability verifications becoming more critical [2]. Furthermore, given that the fatigue strength curves are the same regardless of material grade, fatigue is expected to become more important for hybrid girders as the flange may be subjected to a higher stress compared to non-hybrid girders. The potential and structural behaviour of hybrid I-sections combining

lower and higher strength steel grades has been explored in various studies. An experimental study to investigate the shear capacity of hybrid steel I-girders was presented by Azizinamini et al. [3] and their proposal led to modifications in AASHTO LRFD [4] bridge design specifications such that the shear strength provisions apply equally to both hybrid and homogeneous girders. Chacón et al. [5] examined longitudinally stiffened hybrid steel plate girders and made recommendations for current EN 1993-1-5 [6] formulations. Shokouhian and Shi [7] studied hybrid steel I-sections, focussing on the effect of flange and web slenderness on member ductility, and proposed a continuous design equation to determine their flexural strength [8]. Recently, the rotation capacity of hybrid beams with flanges in Grade S690 and S355 web were investigated through experimental and numerical studies by Bartsch et al. [9].

The application of stainless steels in the construction sector has increased over the last decades due to their distinctive mechanical properties, such as significant strain hardening, high ductility and excellent corrosion resistance. This is of particular importance for structures with long design life such as bridges, which are often exposed to highly corrosive conditions, either due to the proximity to marine environments, or due to the use of de-icing salts, which over time may lead to degradation of structural performance and ultimately the need for costly maintenance. The direct cost associated with inspection and maintenance of bridges is a significant part of their life cycle cost, whilst the indirect cost due to road closures and the resulting delays or disruptions to social and economic activities can be as high as ten times the direct cost. Therefore, the efficiency of bridge designs adopting stainless steels for bridges has been investigated based on whole life costing considerations, and it was concluded that certain high strength grades like lean duplex stainless steels, may lead to significant reduction in overall cost, even when the indirect maintenance cost is not considered [10-12]. In the above studies the stainless steel girders where homogeneous and design was based on relevant design standards. Given the high initial material cost of stainless steels, minimising the material usage via efficient design is warranted. To this end, adopting hybrid stainless steel girders may lead to improved efficiency, as can the application of efficient design methods in ULS verifications, particularly for applications less likely to be governed by fatigue considerations such as footbridges.

The performance of homogeneous stainless steel I-sections has been well investigated through a series of experimental and numerical studies on stub columns and beams [13-16]. The fabrication of hybrid stainless steel I-sections made from different grades for the flanges and the web, is possible through various welding procedures, such as laser welding and shielded metal arc welding. Recently, Lalthazuala and Singh [17-19] presented a numerical study on hybrid stainless steel I-sections in compression and bending and proposed modified EN 1993-1-4 and DSM formulations. The aforementioned study focused only on duplex and lean duplex grades and considered only the application of the Direct Strength Method. Aiming to improve the understanding of the fundamental structural performance of hybrid stainless steel sections and to extend the application of the design

procedures to hybrid sections, the current study presents a numerical investigation on predominantly non-slender I-sections employing different stainless steel grades in the flange and the web. The cross-sectional strength in pure compression and in major axis bending are examined. The experimentally verified finite element model is discussed in Section 2 and a subsequent numerical parametric study is carried out in Section 3. The results are utilised in Section 4 to assess the applicability of the EN 1993-1-4 [20] and to extend the continuous strength method (CSM) [21] to hybrid stainless steel sections in compression and in bending.

2. Numerical modelling

The general-purpose finite element (FE) model package Abaqus [22] was used to generate numerical models in order to simulate the associated structural performance of hybrid stainless steel cross-sections. Stub column and four-point bending models were firstly validated against existing experimental results [13-16] and subsequently used for parametric studies to expand the numerical data over a wide range of section geometries and material combinations. A brief description of the experimental programme is presented in Section 2.1, whilst Sections 2.2 and 2.3 provide information on the development and validation of the FE models, respectively.

2.1. Selected test data

To the author's knowledge, there is no test data available in literature on hybrid stainless steel girders and consequently experiments on conventional homogeneous stainless steel I-sections were used in the present study to validate the numerical models. Experimental studies on austenitic and lean duplex I-sections tested in compression and four-point bending have been reported in [13-16]. Since the present investigation focuses on plate girders in compression and in bending, stub column tests and test data under the major axis bending were considered from these investigations. The selected sections were manufactured by either laser welding [14, 15] or metal arc welding [13,16] of hot rolled steel plates and had sharp edges and corners as shown in Figure 1, where the notation of the section geometry adopted herein is also included. The dimensions and the designations of the tested specimens along with examined stainless steel alloys, the measured imperfections w_0 and the ultimate experimental compression loads ($N_{u,test}$) and moments ($M_{u,test}$) reported in [13-16] are summarised for reference in Tables 1 and 2 for compression and four-point bending, respectively. The stub column length L and plate slenderness of the flange $\bar{\lambda}_{p,f}$ and the web $\bar{\lambda}_{p,w}$ determined in accordance to EN 1993-1-1 [23] and EN 1993-1-5 [6] are also included in these tables. The ratios $N_{u,test}/N_{u,FE}$ and $M_{u,test}/M_{u,FE}$ are explained in section 2.3.

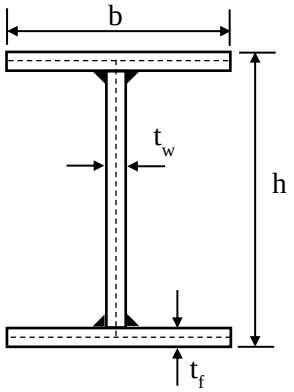

Figure 1: Cross-section geometry and notation of specimens

Table 1: Stub column test data [13-16]

Ref.	**Stainless alloy**	**Specimen**	**L (mm)**	**b (mm)**	**h (mm)**	**t_f (mm)**	**t_w (mm)**	$\bar{\lambda}_{p,f}$	$\bar{\lambda}_{p,w}$	**w_0 (mm)**	**$N_{u,test}$ (kN)**	**$N_{u,test}/N_{u,FE}$**
[13]	Lean Duplex 1.4162	I-200×140×6×6*	600.35	138.9	214.29	6.12	6.01	0.90	0.91	0.35	1473	0.91
		I-200×140×8×6*	600.33	139	217.14	8.04	5.98	0.66	0.91	0.29	1849	0.93
		I-200×140×10×8	600.28	139	219.85	10.35	8.03	0.49	0.65	0.34	2540	0.94
		I-200×140×12×8	600.15	139.3	224.49	12.68	8.14	0.39	0.64	0.27	2978	0.90
[14,15]	Austenitic 1.4307, 1.4404, 1.4571	I-50×50×4×4	150.29	50.49	50.33	3.91	3.99	0.36	0.21	0.23	281.1	0.84
		I-102×68×5×5	304.72	68	101.8	5.11	5.01	0.34	0.33	0.22	429.7	0.93
		I-140×140×10×12	420.32	140.78	139.78	11.82	9.71	0.33	0.23	1.3	2042.2	0.79
		I-150×75×7×10	450.09	75.83	150.46	9.9	7.05	0.21	0.36	0.16	854	1.01
		I-152×160×6×9	456.12	160.57	152.28	8.79	6.18	0.47	0.43	0.34	1163.2	0.95
		I-160×82×10×12	480.19	83.24	159.95	11.72	9.79	0.19	0.27	0.16	1397.5	0.91
		I-203×133×6×8	612.09	133.9	205.08	7.83	5.9	0.50	0.61	0.11	1090.3	0.95
		I-220×110×6×9*	660	110.41	219.6	8.91	6.07	0.36	0.66	0.15	1071.8	0.91
		I-300×150×7×11*	840	150.52	295.16	11.81	6.92	0.37	0.71	0.2	1672.4	0.98
[16]	Austenitic 1.4301	I304-150	449.6	149.5	149.55	10	6	0.48	0.46	0.55	1568.3	0.87
		I304-192*	598	185.25	193.85	6	6	0.98	0.65	1.05	949.4	0.95
		I304-192-a	601.1	126.25	194.2	6	6	0.65	0.65	0.79	859.8	0.91
		I304-252*	779.9	245.7	253.25	6	6	1.30	0.86	1.17	968.8	1.03
		I304-260	779.9	165.7	258.95	10	6	0.53	0.85	0.67	1622.8	0.95
		I304-282*	850.4	185.6	282.9	6	6	0.98	0.97	0.87	905.5	0.99
		I304-312*	951.6	305.5	313.7	6	6	1.63	1.08	1.51	1088.7	1.00
		I304-320	961.6	205.6	319.6	10	6	0.67	1.07	0.71	1804.4	0.96
		I304-372*	1117.8	246.05	373.3	6	6	1.31	1.29	1.2	978.5	1.01
		I304-462*	1400.7	186	462.55	6	6	0.98	1.61	1.11	893.8	1.03
	Duplex 1.4462	I2205-150	449.4	150	150.65	10.2	6	0.62	0.64	0.59	2549.9	1.00
		I2205-192-a*	600	125.8	193.1	6	6	0.90	0.89	0.6	1447.7	0.94
		I2205-200	601.4	124.9	200.55	10.2	6	0.51	0.88	0.71	2298.6	0.94
		I2205-252*	780	245.25	252.85	6	6	1.79	1.18	0.55	1653.2	1.03
		I2205-372*	1117	245	372.85	6	6	1.79	1.77	0.77	1686.3	1.03

*Denotes slender Class 4 section

Table 2: Four-point bending test data [13,15]

Ref.	Stainless alloy	Specimen	Span (mm)	b (mm)	h (mm)	t_f (mm)	t_w (mm)	$\bar{\lambda}_{p,f}$	$\bar{\lambda}_{p,w}$	w_0 (mm)	$M_{u,test}$ (kNm)	$M_{u,test}/M_{u,FE}$
[13]	Lean Duplex 1.4162	I-200×140×6×6-2*	1800	138.6	214.27	6.11	6.01	0.90	0.37	0.35	132	0.92
		I-200×140×8×6-2	1800	139.3	216.82	8.11	6.06	0.66	0.37	0.29	169	0.95
		I-200×140×10×8-2	1800	139	219.79	10.26	7.99	0.49	0.27	0.34	219	0.97
		I-200×140×12×8-2	1800	139.64	223.51	12.32	8.07	0.40	0.26	0.27	259	1.01
[15]	Austenitic 1.4307, 1.4404, 1.4571	I-102×68×5×5	1600	67.98	102.31	5.08	5.03	0.19	0.13	0.22	15.19	0.94
		I-160×82×10×12	1700	83.35	160.26	11.79	9.83	0.08	0.10	0.16	73.04	0.97
		I-50×50×4×4	900	50.52	50.39	3.98	4	0.12	0.08	0.23	4.46	0.99
		I-150×75×7×10	1700	75.9	150.77	9.87	6.92	0.06	0.14	0.16	46.57	0.98

*Denotes slender Class 4 section

The material properties of the specimens tested in compression and bending and obtained from coupon testing in [13-16] are reported in Tables 3 and 4, respectively, where E is the Young's modulus, f_y is the 0.2% proof strength, f_u is the ultimate stress, ε_u is the strain at ultimate stress and n and m and Ramberg-Osgood non-linear parameters. The subindexes "$_f$" and "$_w$" have been added to the above variables to refer to the materials properties of the flange and the web, respectively. Material models for stainless steel have been developed over last decades and are in essence generalisations of the original Ramberg-Osgood material model which offer improved approximations of the experimentally observed material response [24-27].

Table 3: Material data of stub column tests [13-16]

Specimen	E_f (GPa)	$f_{y,f}$ (MPa)	$f_{u,f}$ (MPa)	$\varepsilon_{u,f}$	n_f	m_f	E_w (GPa)	$f_{y,w}$ (MPa)	$f_{u,w}$ (MPa)	$\varepsilon_{u,w}$	n_w	m_w
I-200×140×6×6	193.5	516	727.5	29	10.7	-	193.5	516	727.5	29	10.7	-
I-200×140×8×6	203	504	727.5	31	12.15	-	193.5	516	727.5	29	10.7	-
I-200×140×10×8	216.5	501	768.5	35	11.75	-	203	504	727.5	31	12.2	-
I-200×140×12×8	205.5	456.5	722.5	37	10	-	203	504	727.5	31	12.2	-
I-50×50×4×4	190.7	270	694	61	4	3	190.7	270	694	61	4	3
I-102×68×5×5	186.8	222	580	50	3.2	3.8	186.8	222	580	50	3.2	3.8
I-140×140×10×12	193.7	272	615	50	7.1	2.6	186.8	260	617	55	7	2.5
I-150×75×7×10	197.3	274	596	58	5	3	197.2	267	560	50	5	2.7
I-152×160×6×9	204.7	227	561	52	6	2.8	191.4	272	586	50	5.2	3.2
I-160×82×10×12	197.5	286	619	52	7.5	2.5	198.5	264	618	53	5.2	3.1
I-203×133×6×8	192.5	281	597	47	4.2	3.3	192.5	251	576	55	4.1	2.9
I-220×110×6×9	197.2	292	671	55	6.2	2.6	193	275	670	61	6	2.8
I-300×150×7×11	196.5	290	589	45	5.8	2.6	200.6	237	581	55	5.6	3
I304-150	188.8	328.5	659.8	50.2	6.9	2.4	188.6	312.6	695.7	55	5.8	2.3
I304-192	188.6	312.6	695.7	55.1	5.8	2.3	188.6	312.6	695.7	55	5.8	2.3
I304-192-a	188.6	312.6	695.7	55.1	5.8	2.3	188.6	312.6	695.7	55	5.8	2.3
I304-252	188.6	312.6	695.7	55.1	5.8	2.3	188.6	312.6	695.7	55	5.8	2.3
I304-260	188.8	328.5	659.8	50.2	6.9	2.4	188.6	312.6	695.7	55	5.8	2.3
I304-282	188.6	312.6	695.7	55.1	5.8	2.3	188.6	312.6	695.7	55	5.8	2.3
I304-312	188.6	312.6	695.7	55.1	5.8	2.3	188.6	312.6	695.7	55	5.8	2.3
I304-320	188.8	328.5	659.8	50.2	6.9	2.4	188.6	312.6	695.7	55	5.8	2.3
I304-372	188.6	312.6	695.7	55.1	5.8	2.3	188.6	312.6	695.7	55	5.8	2.3
I304-462	188.6	312.6	695.7	55.1	5.8	2.3	188.6	312.6	695.7	55	5.8	2.3
I2205-150	191.2	574.8	775	20.6	6.7	3.1	193.2	605.6	797.9	21	7.4	3.1
I2205-192-a	193.2	605.6	797.9	21	7.4	3.1	193.2	605.6	797.9	21	7.4	3.1
I2205-200	191.2	574.8	775	20.6	6.7	3.1	193.2	605.6	797.9	21	7.4	3.1
I2205-252	193.2	605.6	797.9	21	7.4	3.1	193.2	605.6	797.9	21	7.4	3.1
I2205-372	193.2	605.6	797.9	21	7.4	3.1	193.2	605.6	797.9	21	7.4	3.1

Table 4: Material data of four-point bending tests [13,15]

Specimen	E_f (GPa)	$f_{y,f}$ (MPa)	$f_{u,f}$ (MPa)	$\varepsilon_{u,f}$	n_f	m_f	E_w (GPa)	$f_{y,w}$ (MPa)	$f_{u,w}$ (MPa)	$\varepsilon_{u,w}$	n_w	m_w
I-200×140×6×6-2	193.5	516	747.5	40	10.7	2.15	193.5	516	747.5	40	10.7	2.15
I-200×140×8×6-2	203	504	737	31	12.2	2.2	193.5	516	747.5	40	10.7	2.15
I-200×140×10×8-2	216.5	501	770	35	11.8	2.25	203	504	737	32	12.2	2.2
I-200×140×12×8-2	205.5	456.5	722.5	36	10	2.4	203	504	737	32	12.2	2.2
I-102×68×5×5	186.8	222	580	50	3.2	3.8	186.8	222	580	50	3.2	3.8
I-160×82×10×12	197.5	286	619	52	7.5	2.5	198.5	264	618	53	5	3.1
I-50×50×4×4	190.7	270	694	61	4	3	190.7	270	694	61	4	3
I-150×75×7×10	197.2	267	560	50	5	2.7	197.3	274	596	58	5	3

2.2. Modelling assumptions

The geometry of the specimens selected for the development of the FE model from [13-16] was discretised using the four-noded multi purpose shell element with reduced integration and finite membrane strains S4R. This type of element has been widely and successfully used in several numerical investigations involving both stainless steel [28-35] and I-section plate girders [5,36,37]. The models were based on centreline dimensions shown by the dash lines in Figure 1. Mesh convergence studies were conducted to determine an appropriate mesh density to achieve suitably accurate results while minimising computational time. On this basis, the models were discretised with a uniform mesh of an element size approximately equal to the plate thickness.

The numerical model developed for compression tests (stub columns) is shown in Figure 2. Kinematic coupling constraints were employed at the top edge of the I-sections and symmetry of the problem was exploited by modelling one quarter of the I-section geometry and applying symmetric boundary conditions. A compression load was applied at the controlling reference point of the kinematic coupling constraint. Figure 3 shows the model developed for beams loaded in four-point bending highlighting the boundary conditions and interactions. The load was applied at the reference points controlling the coupling at the loading sections.

Stainless steel material nonlinearity was modelled by using the von Mises yield criterion with isotropic hardening. Using the material properties from Tables 3 and 4 reported in [13-16], full stress-strain curves were generated using the modified compounds two-stage Ramberg-Osgood model [24,25] included in Annex C of EN 1993-1-4 [20]. The generated curves, which are defined in terms of engineering stress σ_{eng} and strain ε_{eng} , were converted into true stresses σ_{true} and logarithmic plastic strains $\varepsilon_{pl,true}$ by using Eqs. (1) and (2) and implemented in the FE model.

$$\sigma_{true} = \sigma_{eng}(1 + \varepsilon_{eng}) \quad (1)$$

$$\varepsilon_{pl,true} = ln(1 + \varepsilon_{eng}) - \frac{\sigma_{true}}{E} \quad (2)$$

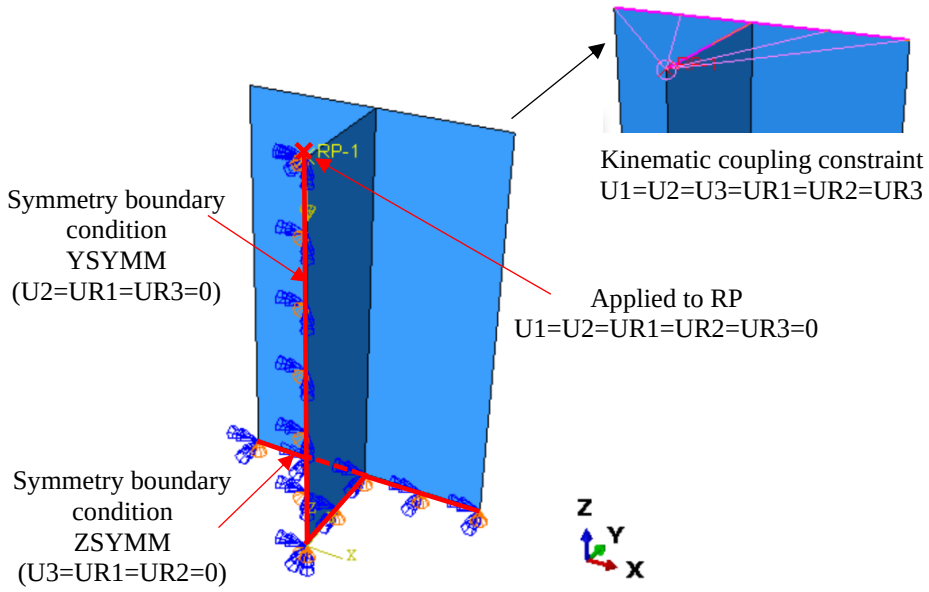

Figure 2: Boundary conditions and constrains used in stub column models

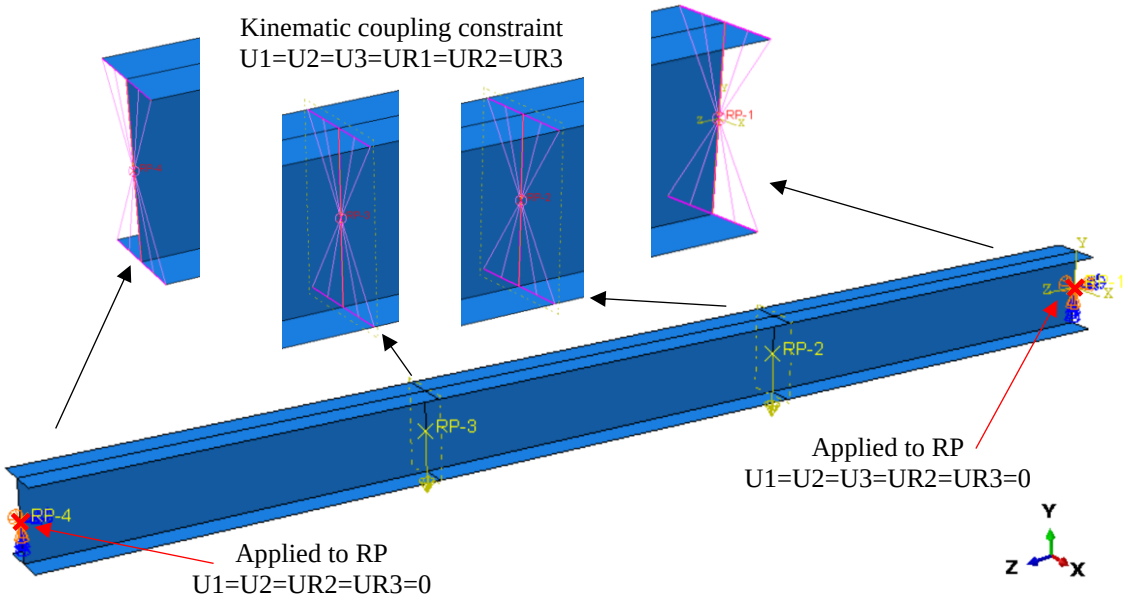

Figure 3: Boundary conditions and constrains used in four-point bending models

Residual stresses in various stainless steel cross-sections manufactured with different processes has been investigated [38-41]. In the FE model developed herein residual stresses have been not included as they have little impact on the compression and bending response of the cross-sections both used in the development of the FE model and subsequently in the parametric study. In addition to this, because residual stress data on hybrid stainless steel I-sections does not exist it was deemed more suitable to neglect them for consistency. Initial geometric imperfections were incorporated into the FE models in the form of the buckling mode shape corresponding to the lowest symmetric elastic critical buckling load. As presented in the following section, various imperfection amplitudes were considered. To

accurately trace the pre- and post- buckling response of the models, static analysis using the modified Riks procedure and taking into consideration both material and geometric nonlinearities was used.

2.3. Validation of the model

The accuracy of the developed FE models to replicate the ultimate response and physical behaviour was assessed by comparing the ultimate compression loads $N_{u,test}$ and bending moments $M_{u,test}$ achieved through testing in [13-16] against the equivalent numerical values $N_{u,FE}$ and $M_{u,FE}$ predicted by the FE models. The comparison is presented in Tables 5 and 6 in terms of the mean of the numerical-to-experimental ratio and coefficient of variation (COV) for various data sets and initial imperfections. Four imperfection magnitudes were considered: $t_f/100$, b/200, the expression given by Eq. (3) proposed by Dawson and Walker (D&W) [42,43] and the actual measured imperfection w_0 reported in Tables 1 and 2. In Eq. (3) t is the plate thickness, f_y is the material 0.2% proof stress and σ_{cr} is the elastic buckling stress of the cross-section plate elements assuming simply supported conditions. For I-sections, the σ_{cr} of the flange and the web was first evaluated to determine the controlling element (i.e. whichever was smaller). To find $w_{0,D\&W}$, the lowest σ_{cr} of either the flange and the web along with f_y and t of the controlling element was used.

$$w_{0,D\&W} = 0.023\left(\frac{f_y}{\sigma_{cr}}\right)t \tag{3}$$

Based on the results reported in Table 5 for the measured geometric imperfection w_0, it is observed a fairly good agreement between the test and numerical data with mean values close to unity and relatively low coefficient of variation (COV). The test to numerical ratios for both stub columns $N_{u,exp}/N_{u,FE}$ and bending tests $M_{u,exp}/M_{u,FE}$ obtained for the measured geometric imperfection w_0 aare reported in Tables 1 and 2, respectively. For the parametric study, the imperfection magnitude model $t_f/100$ is selected as it provides very similar results to that predicted when the measured imperfection is used. The fact that Dawson and Walker imperfection provided the least agreement is because the predicted imperfection magnitudes by Eq. (3) were one order of magnitude smaller than the others thereby resulting in higher numerical values and hence higher mean values. Typical experimental and numerical failure modes are presented in Figure 4 which demonstrates close agreement and the ability of the FE to replicate physical behaviour of I-sections subjected to compression and to four-point bending. In Figure 5 a comparison of the load against end shortening for stub column test I2205-372 [16] is shown utilising imperfection amplitude w_0 which shows that the numerical model is able to accurately capture pre and post-buckling response.

Table 5. Comparison between experimental and FE ultimate compression loads

Data set		$N_{u,FE}/N_{u,test}$			
		Imperfection magnitude			
		$t_f/100$	b/200	$w_{0D\&W}$	w_0
[13]	Mean	0.96	0.90	0.96	0.93
	COV	0.026	0.021	0.018	0.019
[14,15]	Mean	0.94	0.90	1.08	0.92
	COV	0.058	0.059	0.165	0.073
[16]	Mean	1.02	0.98	1.23	0.98
	COV	0.046	0.050	0.221	0.050
Lean Duplex [13,16]	Mean	0.98	0.95	1.12	0.96
	COV	0.037	0.059	0.226	0.049
Austenitic [14-16]	Mean	0.98	0.94	1.15	0.95
	COV	0.069	0.068	0.211	0.068
All	Mean	0.98	0.94	1.14	0.95
	COV	0.060	0.065	0.212	0.062

Table 6. Comparison between experimental and FE ultimate bending loads

Data set		$M_{u,FE}/M_{u,test}$			
		Imperfection magnitude			
		$t_f/100$	b/200	$w_{0D\&W}$	w_0
Lean Duplex [13]	Mean	0.97	0.95	0.96	0.96
	COV	0.041	0.041	0.039	0.039
Austenitic [15]	Mean	0.97	0.97	0.97	0.97
	COV	0.023	0.018	0.027	0.021
All	Mean	0.97	0.96	0.96	0.97
	COV	0.031	0.030	0.032	0.029

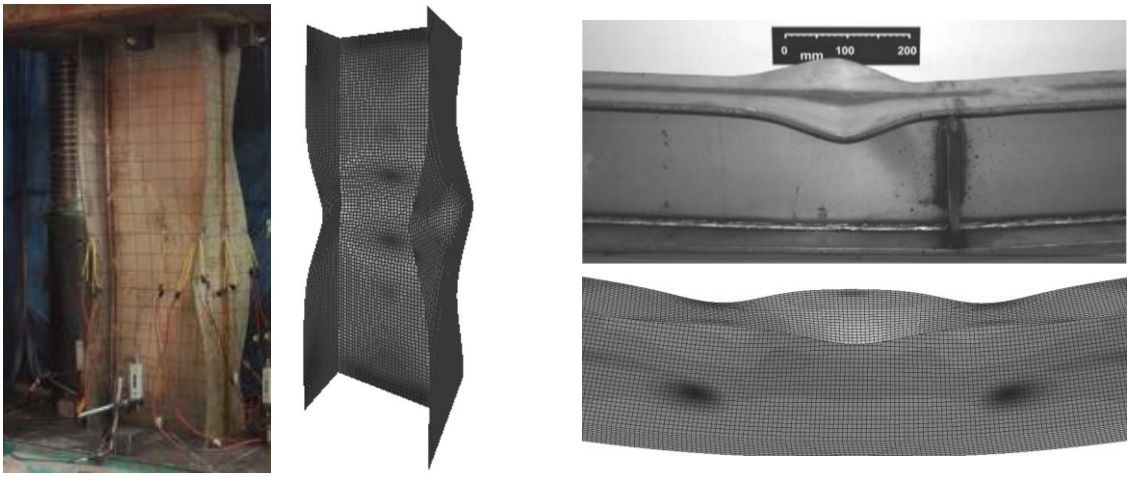

a) Specimen I2205-372 [16] b) Specimen I-200×140×8×6-1 [13]

Figure 4: Comparison between experimental and numerical failure modes

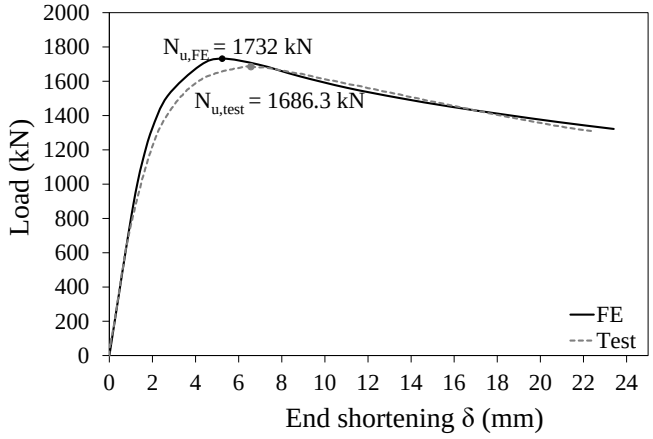

Figure 5: Experimental and numerical response of stub column I2205-372 [16]

3. Parametric study

3.1. Hybrid combinations used in the present study

Having validated the numerical model, a parametric study was undertaken to investigate the structural behaviour of hybrid stainless steel I-sections subjected to compression and to major axis bending under the four-point configuration. The list of parameters considered is presented in Table 7. Three cross-sectional aspect ratios h_w/b and five flange thicknesses t_f were examined which were combined with ten web thicknesses. The generated models covered all cross-sectional classes, determined according to EN 1993-1-4 [20]. Note that Eurocode adopts the cross-section classification framework in order to consider local buckling effect on the cross-section structural response. In this study, the flanges of the models in compression were Class 1 to 4 while the flange of the models in bending were either Class 1 or 2. The class of the webs of both models in compression and in bending ranged from 1 to 4.

Any structural member exposed to temperature changes will be subjected to thermal strains, which may generate significant thermal stresses, if the thermal expansion or contraction is restrained. For hybrid sections comprising plates with different coefficients of thermal expansion, such a restrain exists along the welded edges of the plates and hence self-equilibrating thermal stresses will develop within the hybrid section due to changes in temperature, thus decreasing both the strength and the fatigue life of such girders. Therefore, hybrid girders should comprise plates having the same coefficient of thermal expansion. According to EN 1993-1-2 [44] and the Design manual for structural stainless steel [45] the coefficient of thermal expansion varies significantly among the three main families of structural stainless steel grades, but remains the same for the various alloys belonging to the same stainless steel family (i.e. austenitic, ferritic, duplex). Hence, in this study, the hybrid stainless steel sections considered employ stainless steel grades within the same family of grades. Other compatibility aspects such as weldability, microstructural stability, chemical composition, galvanic corrosion and cost benefit are out of scope in the present investigation.

The combination of material grades considered is shown in Table 7 with material properties given in Table 8; the material grades result in the maximum possible variation in yield strengths within the stainless steel grade family considered. Ferritic grade combinations were not considered, due to the unavailability of ferritic stainless steel plates with significant differences in yield strength. In all cases the higher material grade is assigned to the flanges and the lower to the web, as customarily done for carbon steel plate girders. Note that in Table 8 m and ε_u are based on predictive models and calculated via the equations included in Table 8. A total number of 240 models were generated, 120 FE models in compression and 120 models in four-point bending. Of these, half were models of hybrid sections, with the remaining being homogeneous sections used as benchmarks.

Table 7: Parameters varied in the parametric study

Parameter	**Value**
3 aspect ratios ($h_w \times b$)	1 (100×100) 1.5 (150×100) 2 (200×100)
5 flange thickness t_f (mm)	5, 6, 8, 10, 12
10 web thickness t_w (mm)	5, 6, 8, 10, 12 (t_f/t_w = 1) 3.5, 4.2, 5.6, 7, 8.4 (t_f/t_w = 1.43)
4 stainless steel grades	2 Austenitics: 1.4307 and 1.4318 2 Duplex: 1.4362 and 1.4662
2 homogeneous combinations (flange-web)	1.4307-1.4307, 1.4362-1.4362
2 hybrid combinations (flange-web)	1.4318-1.4307 (f_{yf}/f_{yw}=1.65) 1.4662-1.4362 (f_{yf}/f_{yw}=1.2)

Table 8: Material properties for parametric study

Alloy	Grade	α (10^{-6}/°C)	E (GPa)	f_y (MPa)	f_u (MPa)	n	m[a]	ε_u[b]
Austenitic	1.4307	16	200	200	500	6.00	2.40	0.60
	1.4318	16	200	330	630	6.00	2.83	0.48
Duplex	1.4362	13	200	400	630	5.00	3.22	0.37
	1.4662	13	200	480	680	5.00	3.47	0.29

[a] $m=1+3.5(f_y/f_u)$
[b] $\varepsilon_u=1-(f_y/f_u)$

4. Results and discussion

4.1. Assessment of EN 1993-1-4 design provisions

Based on the results of the parametric study, the design provisions of EN 1993-1-4 [20] for stainless steel elements in compression and in bending are assessed. To this end, the results are analysed and the critical (i.e. most slender) element among the flange and the web is determined, by comparing their non-dimensional slenderness $\bar{\lambda}_p$. For all simulated sections in bending, the flange was the most slender element, whilst for the cross-sections in compression, the critical element was the flange for the sections with an aspect ratio of 1 and for the sections with aspect ratio 1.5 and 2 the critical element was the web.

In Figure 6, the ratio of the numerically obtained compression resistance $N_{u,FE}$ over the cross-section yield load N_y, determined as the sum of the yield load of the flanges and the web, is plotted against the slenderness parameter (i.e. c/tε where c is the flat part of the element and $\varepsilon = \sqrt{(235/fy)(E/210)}$ as defined in EN 1993-1-4 [20]) of the flange for both homogeneous and hybrid sections for which the flange was the most slender element. The results are presented separately for homogeneous and hybrid sections and for the examined stainless steel grades. A very strong trend can be observed with all points being narrowly grouped together and displaying a reduction in compression resistance with increasing flange slenderness. No significant difference can be observed between the homogeneous and the hybrid sections, whilst the slenderness limit of 14 [20,46] for outstand members in compression appears suitable, with the points at or near this limit achieving marginally higher compression resistances than their squash load. A similar graph for the assessment of the slenderness limit of internal elements in compression, is shown in Figure 7. Again, no significant difference in the observed responses exists between homogeneous and hybrid sections and the slenderness limit of 37 for internal elements in compression is suitable.

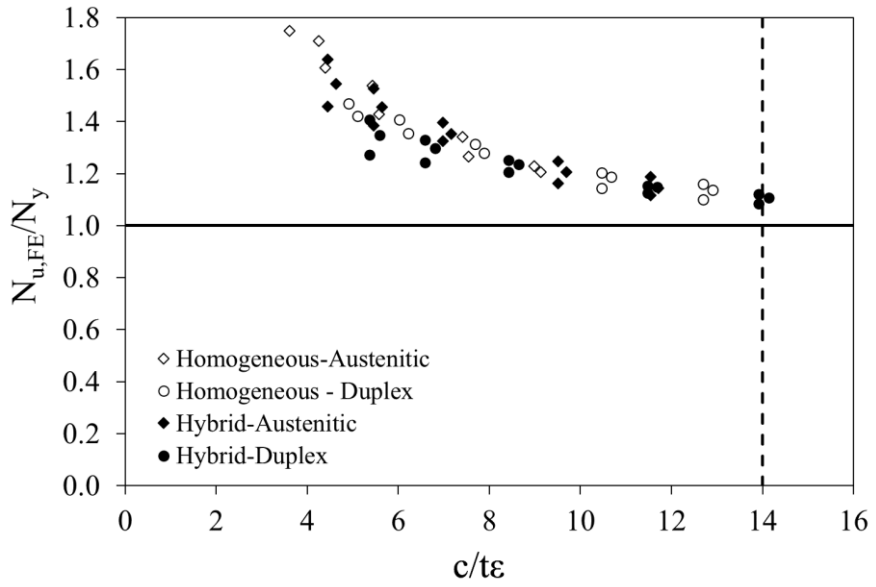

Figure 6: Assessment of Class 3 slenderness limit for outstand elements in compression, based on stub column results

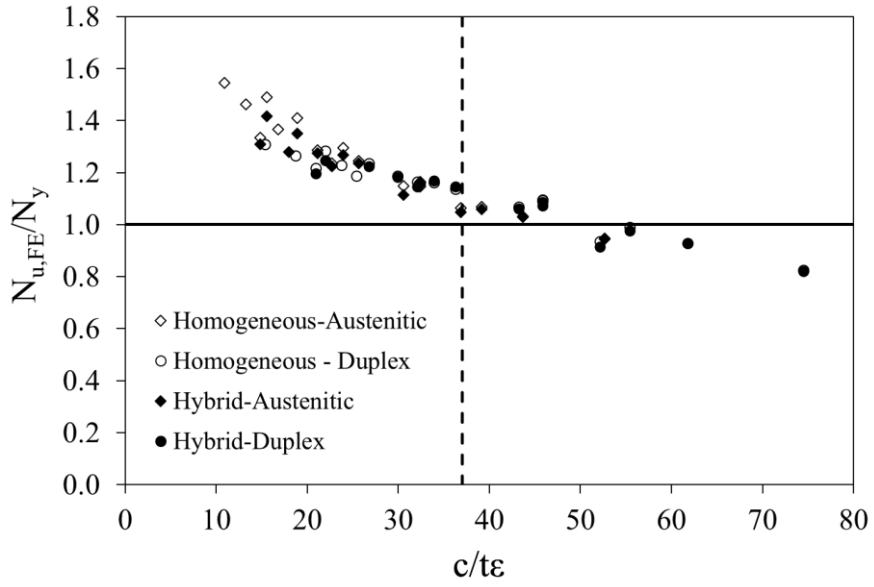

Figure 7: Assessment of Class 3 slenderness limit for internal elements in compression, based on stub column results

Based on the results of the simulated flexural members, the Class 3 and the Class 2 slenderness limits for outstand elements in compression are assessed by plotting the slenderness parameter c/tε against the numerically obtained moment resistance normalised by the elastic moment resistance M_{el} and plastic moment resistance M_{pl} respectively. As before, the moment resistance of the hybrid sections was obtained as the sum of the moment resistances of their respective cross-section elements. In Figure 8, the Class 3 limit of outstand elements in compression is assessed based on the numerical results of the simulated beam sections. The Class 3 limit of 14 still appears safe based on the bending simulations, however, compared to Figure 7, where the same is assessed based on stub column results, a higher scatter of the results can be observed, particularly with decreasing slenderness. The increased scatter is arguably due to the increasing importance of material strain hardening for stocky sections combined with the added complexity of the varying stress distribution through the web, which is only linear near the attainment of M_{el} and becomes increasingly nonlinear with decreasing slenderness. Thus, M_{el} by which the moment resistance of all models is normalised, is less relevant for the stocky region of the plot. The Class 1 limit has not been assessed, since it is well known to display significant scatter [30] and to depend on additional parameters such as the beam moment gradient, which have not been considered in this study.

The FE results of both the stub columns and the beams have also been utilised to assess the applicability of EN 1993-1-4 cross-section strength predictions to stainless steel hybrid plate girders. The numerically obtained strengths are compared with the cross-section compression and flexural design predictions evaluated according to EN 1993-1-4 and the results are presented in Tables 9 and 10, respectively, and will be discussed in the following section.

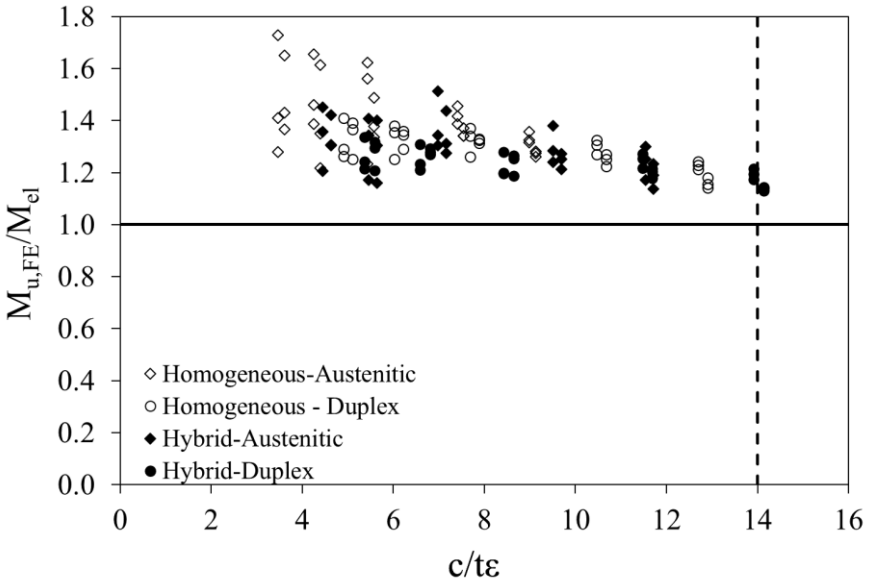

Figure 8: Assessment of Class 3 slenderness limit for outstand element in compression, based on flexural results

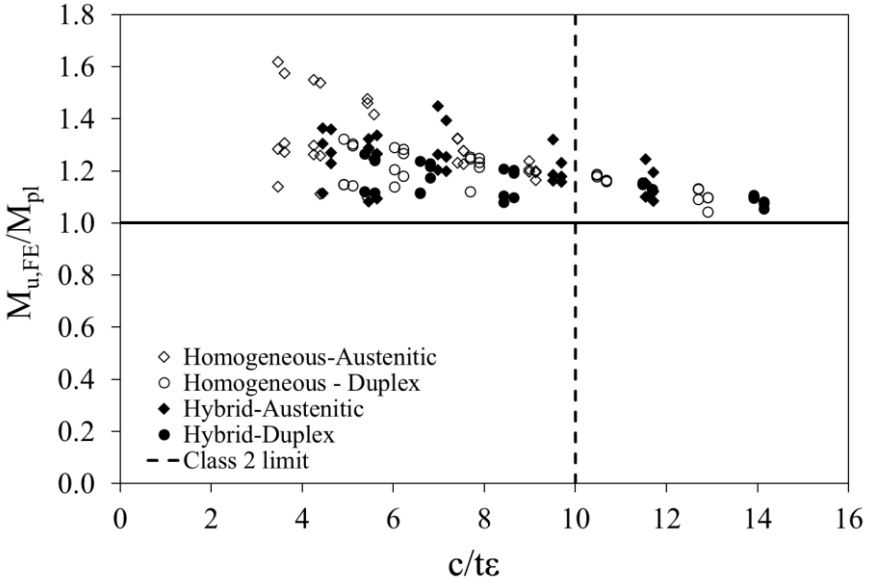

Figure 9: Assessment of Class 2 slenderness limit for outstand element in compression, based on flexural results

4.2. Extension of the Continuous Strength Method to hybrid girders

The results of the parametric study were also used to extend the continuous strength method (CSM) [21,47] for application to hybrid stainless steel I-sections. The CSM is a deformation based design method that allows better exploitation of stainless steel's material strain hardening and employs the following elements: (1) a base curve given in Eqs. (4) and (5) and a bi-linear material model given in Eqs. (8-10). The CSM was originally developed to cover stocky cross-sections (i.e. $\bar{\lambda}_p \leq 0.68$, Eq. (4)) and has been recently extended by [48] to cover slender cross-sections, Eq. (5). The CSM design equations for the fundamental cases of compression and bending about the major axis are given in Eqs. (16) and (17) where A is the cross-sectional area and $W_{el,y}$ and $W_{pl,y}$ are the elastic and plastic section modulus, respectively, about the strong axis.

For $\bar{\lambda}_p \leq 0.68$ $\quad \frac{\varepsilon_{csm}}{\varepsilon_y} = \frac{0.25}{\bar{\lambda}_p^{3.6}}$ but $\quad \frac{\varepsilon_{csm}}{\varepsilon_y} \leq min\left(15, \frac{C_1 \varepsilon_u}{\varepsilon_y}\right)$ (4)

For $\bar{\lambda}_p > 0.68$ $\quad \frac{\varepsilon_{csm}}{\varepsilon_y} = \left(1 - \frac{0.222}{\bar{\lambda}_p^{1.050}}\right) \frac{1}{\bar{\lambda}_p^{1.050}}$ (5)

Where, $\quad \bar{\lambda}_p = \sqrt{\frac{f_y}{\sigma_{cr}}}$ (6)

C_1= 0.1 for austenitic and duplex grades
C_1=0.4 for ferritic grades (7)

In Eqs. (4) and (5) $\varepsilon_{csm}/\varepsilon_y$ is the normalised cross-section deformation, where $\varepsilon_y=f_y/E$, and is a continuous function of the cross-section slenderness, $\overline{\lambda}_p$. In Eq. (6), σ_{cr} is the elastic buckling stress of either the full cross-section or its most slender constituent plate element.

$$f_{csm} = f_y + E_{sh}\varepsilon_y\left(\frac{\varepsilon_{csm}}{\varepsilon_y} - 1\right) \quad (8)$$

$E_{sh} = \frac{f_u - f_y}{0.16\varepsilon_u - \varepsilon_y}$ for austenitic and duplex stainless steel (9)

$E_{sh} = \frac{f_u - f_y}{0.45\varepsilon_u - \varepsilon_y}$ for ferritic stainless steel (10)

In Eq. (8), f_{csm} is the CSM stress and E_{sh} is the material strain hardening slope which has different equations for austenitic and duplex alloys, Eq. (9), and ferritic alloys, Eq. (10).

From the stub-column FE results, the ultimate deformation $\delta_{u,FE}$ at ultimate compression load $N_{u,FE}$ was used to determine the cross-sectional deformation capacity $\varepsilon_{csm}/\varepsilon_y$ according to [47], and was plotted against $\bar{\lambda}_p$ as shown in Figure 10. For the determination of $\bar{\lambda}_p$ in the present study, σ_{cr} was determined using the Constrained Finite Strip Method (CUFSM) software [49] to account for element interaction, whilst for the yield strength, which features both in the definition of the non-dimensional slenderness, ε_y and E_{sh} and is not constant in hybrid sections, an effective yield strength $f_{y,eff,A}$ was adopted based on weighted average of the yield strengths of the flange and the web, the weights being the areas of the flanges A_f and the web A_w, respectively, as shown in Eq. (11). The same approach was followed by [19] in their assessment of the Direct Strength Method. It should be noted that in addition to the yield strength, the weighted average approach can be used to obtain all required material properties, like the strain-hardening slope E_{sh} and elastic deformation ε_y from the respective properties of the flanges and the web. Eqs (12) and (13) are the effective weighted variables for ε_y and E_{sh} namely $\varepsilon_{y,eff}$ and $E_{sh,eff}$, respectively, incorporating the effective yield strength. The results for compression data presented in Figure 10 show that hybrid sections follow very closely the existing CSM base curve and overlap with

the data from the homogeneous sections, which demonstrates the applicability of the CSM base curve to hybrid stainless steel sections in compression.

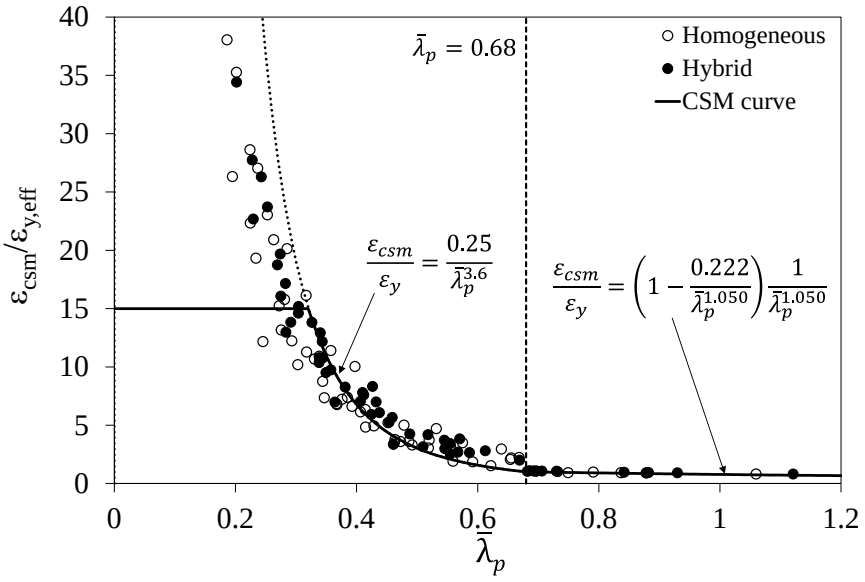

Figure 10: Relationship between deformation capacity and slenderness – compression models

$$f_{y,eff,A} = \frac{f_{y,f}A_f + f_{y,w}A_w}{A} \tag{11}$$

$$\varepsilon_{y,eff} = \frac{\varepsilon_{y,f}A_f + \varepsilon_{y,w}A_w}{A} \tag{12}$$

$$E_{sh,eff} = \frac{E_{sh,f}A_f + E_{sh,w}A_w}{A} \tag{13}$$

Similarly, the ultimate curvature $\kappa_{u,FE}$ at ultimate bending moment $M_{u,FE}$ was used to determine the cross-sectional deformation capacity $\varepsilon_{csm}/\varepsilon_y$ according to [47]. As before, the issue of employing a representative or effective yield strength for hybrid sections emerges. Contrary to the fundamental case of compression, for which a weighted average based on cross-sectional areas is the only reasonable approach, for the case of bending, a number of alternatives for the definition of the effective strength exists. These include using the cross-sectional areas (Eq. (11)), elastic section modulus or the plastic section modulus of the flanges and the web as the weights of the weighted average effective yield strength $f_{y,eff}$, as defined in Eqs. (14) and (15), respectively, where $W_{el,f}$, $W_{el,w}$, $W_{pl,f}$ and $W_{pl,w}$ are the elastic section modulus of the flange, the elastic section modulus of the web, the plastic section modulus of the flange and the plastic section modulus of the web, respectively.

$$f_{y,eff,Wel} = \frac{f_{y,f}W_{el,f} + f_{y,w}W_{el,w}}{W_{el}} \tag{14}$$

$$f_{y,eff,Wpl} = \frac{f_{y,f}W_{pl,f} + f_{y,w}W_{pl,w}}{W_{pl}} \tag{15}$$

For simplicity and to maintain consistency with the fundamental loading case of compression, Eq. (11) is employed for the determination of the effective yield strength. The effect of employing different weights for the weighted average of the yield strength will be investigated later on based on the resulting accuracy in predicting the cross-section resistance. Figure 11 displays the normalised deformation capacity obtained from the FE flexural models against the cross-section slenderness. The base curve is extended to cover slender sections as well, although all of the models had a cross-section slenderness smaller than 0.68. As for the case of compression, the base curve seems to provide a reasonably good fit to the numerically obtained deformation capacities in bending for both homogeneous and hybrid girders.

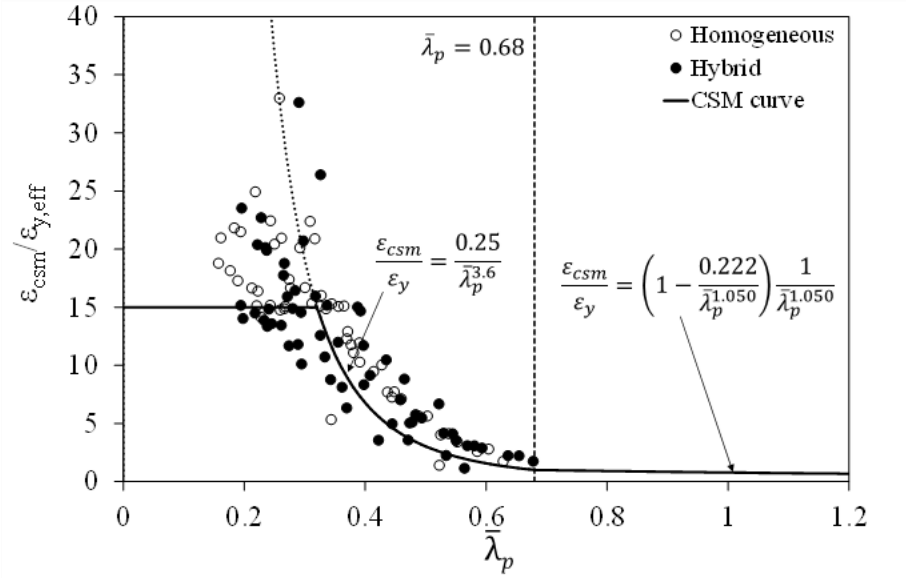

Figure 11: Relationship between deformation capacity and slenderness – bending models

Finally, the CSM is used to predict the cross-section capacity of the modelled cross-sections in compression and in bending. Eq. (4) (replacing ε for $\varepsilon_{y,eff}$) is used to predict the deformation capacity for each modelled section from its non-dimensional slenderness and thereafter Eq. (16) is used to predict the compressive resistance of stub columns models (N_{csm}) and Eq. (17) is used to predict the flexural resistance of the beams ($M_{y,csm}$). In Table 9, the average and coefficient of variation (COV) of the ratio of predicted over numerical compressive resistance $N_{u,pred}/N_{u,FE}$ is reported for all stub column models. To facilitate the assessment of the accuracy of the method, the numerical data have been grouped according to material grade and to whether the section is homogeneous or hybrid, whilst both the CSM and the EN 1993-1-4 methods are assessed. It can be observed that the CSM leads to more favourable strength predictions and smaller COV compared to the EN 1993-1-4 design approach. Equally important is the fact that the CSM predictions for hybrid sections are at least as good as the predictions for the homogeneous sections and display marginally smaller scatter, thus verifying the suitability of the CSM for the prediction of the compressive resistance of hybrid I-sections.

$$N_{csm} = Af_{y,eff,A} + E_{sh,eff}\varepsilon_{y,eff}\left(\frac{\varepsilon_{csm}}{\varepsilon_{y,eff}} - 1\right) \quad (16)$$

$$M_{csm} = W_{pl}f_{y,eff}\left[1 + \frac{E_{sh,eff}}{E_{eff}}\frac{W_{el}}{W_{pl}}\left(\frac{\varepsilon_{csm}}{\varepsilon_{y,eff}} - 1\right) - \left(1 - \frac{W_{el}}{W_{pl}}\right)\Big/\left(\frac{\varepsilon_{csm}}{\varepsilon_{y,eff}}\right)^2\right] \quad (17)$$

Table 9: Assessment of CSM and EN 1993-1-4 predictions for compression $N_{u,pred}/N_{u,FE}$

Grade	Section	CSM		EN 1993-1-4	
		MEAN	COV	MEAN	COV
Austenitic	homogeneous	1.07	0.10	0.77	0.15
	hybrid	1.03	0.10	0.80	0.12
Duplex	homogeneous	0.98	0.07	0.83	0.09
	hybrid	0.97	0.07	0.85	0.08
All homogeneous		1.02	0.10	0.80	0.12
All hybrid		1.00	0.09	0.82	0.11
All		1.01	0.09	0.81	0.12

The design predictions of both CSM and EN 1993-1-4 are assessed based on the obtained FE beam results using the mean and COV of $M_{u,pred}/M_{u,FE}$ ratios in Table 10. To assess the suitability of the various approaches available for obtaining $f_{y,eff}$ defined in Eqs. (11,14,15), the CSM has been assessed for all three cases. As shown in Table 10, the CSM leads to more efficient and on average more accurate predictions of the flexural resistance compared to the EN 1993-1-4 approach. Furthermore, it can be observed that there is no real difference in the accuracy of the CSM regardless which weighted average formulation is used. This can be attributed to both the relatively small difference of the yield strengths considered for the flange and the web (the ratio of yield strength is 1.65 for austenitic stainless steel and only 1.20 for duplex stainless steels) and to the fact that increasing effective yield strength leads to higher cross-section slenderness and hence to a decreased utilisation of its strain-hardening according to the CSM formulation. Thus, over- or under-estimations of the effective yield strength are leading to under- or over-predictions of the section deformation capacity respectively; these two competing effects largely cancel each other out and do not markedly alter the strength predictions. This was verified via additional FE analyses which employed material grades with significantly more different yield strength values. These models, although unrealistic since the combined materials were incompatible in terms of thermal expansion, proved that Eqs. (11, 14, 15) lead to virtually identical strength predictions. Therefore, to maintain consistency with the CSM for compression and for simplicity it is proposed that the effective material properties of a hybrid stainless steel I-section are determined using $f_{y,eff,A}$ given in Eq.(11).

Table 10: Assessment of CSM and EN 1993-1-4 predictions for bending $M_{u,pred}/M_{u,FE}$

Grade	Section	CSM – Eq. (11)		CSM – Eq. (14)		CSM – Eq. (15)		EN 1993-1-4	
		MEAN	COV	MEAN	COV	MEAN	COV	MEAN	COV
Austenitic	homogeneous	0.91	0.09	0.91	0.09	0.91	0.09	0.78	0.10
	hybrid	0.96	0.08	0.96	0.08	0.96	0.08	0.81	0.07
Duplex	homogeneous	0.97	0.08	0.97	0.08	0.97	0.08	0.82	0.05
	hybrid	1.00	0.09	0.99	0.10	0.99	0.09	0.85	0.05
All homogeneous		0.94	0.09	0.94	0.09	0.94	0.09	0.80	0.08
All hybrid		0.98	0.09	0.98	0.09	0.98	0.09	0.83	0.07
All		0.96	0.09	0.96	0.09	0.96	0.09	0.81	0.08

5. Conclusions and future lines of investigation

This paper presented the development and validation of an FE model for stainless steel I-sections in compression and in bending. In absence of published experimental results on hybrid stainless steel I-sections, the validation was based on experimental results on homogeneous welded I-sections. Thereafter a comprehensive parametric study was conducted which included hybrid stainless steel I-girders as well as homogenous ones as benchmark models. The material combinations used for the flanges and the webs of the hybrid girders were carefully selected such that the coefficient of thermal expansion of the material grades is compatible and hence no thermal stresses are expected to develop in the resulting member. The following flange – web hybrid combinations were considered: 1.4318-1.4307 (f_{yf}/f_{yw}=1.65) and 1.4662-1.4362 (f_{yf}/f_{yw}=1.2).

Based on the obtained results, the EN 1993-1-4 slenderness limits for Class 3 and Class 2 for outstand elements in compression and the Class 3 limit for internal elements in compression were assessed and found adequate for the modelled hybrid sections. Furthermore, the CSM was extended, for the first time, to cover hybrid stainless steel I-sections via the adoption of an effective stress and equivalent effective material properties obtained as the weighted average values of the respective values for the flange and the web. Three different weighting methods were explored, and it was concluded that they all yield identical results. Hence it is recommended that for both compression and bending, the material properties are obtained using the areas of the flanges and the web as the weighting factors. Finally, it was shown that in all cases the CSM predictions for hybrid sections were at least as accurate if not more accurate than the predictions for their homogenous counterparts.

Due to thermal expansion compatibility, it is unknown if other hybrid combinations are structurally viable. Apart from that, other compatibility aspects such as weldability, microstructural stability, chemical composition, galvanic corrosion and cost benefit are yet to be investigated. Future hybrid combinations to consider could be:

- Duplex in the flanges and ferritic in the web: this combination will yield the maximum difference in the coefficient of thermal expansion and is a combination for application where stronger flanges are needed due to structural demands such as bridges.

- Austenitic in the flanges and ferritic in the web: for combinations where higher ductility than in a duplex-ferritic combination is required.
- Higher alloy austenitic (1.4401) with lower allow austenitic (1.4301): this is a cost effective combination for applications where only the higher alloy austenitic part is exposed to external conditions.
- Ferritic flanges such as grades (1.4006) and (1.4005) with austenitic web for flanges of a beam with high magnetic permeability.

References

[1] Iles D.C., 2014. SCI Publication P356. Composite Highway Bridge Design.

[2] Veljkovic, M. and Johansson, B., 2004. Design of hybrid steel girders. Journal of Constructional Steel Research, 60(3-5), pp.535-547.

[3] Azizinamini, A., Hash, J.B., Yakel, A.J. and Farimani, R., 2007. Shear capacity of hybrid plate girders. Journal of Bridge Engineering, 12(5), pp.535-543.

[4] AASHTO., 2004. LRFD bridge design specifications, 3rd Ed., Washington, D.C.

[5] Chacón, R., Bock, M. and Real, E., 2011. Longitudinally stiffened hybrid steel plate girders subjected to patch loading. Journal of Constructional Steel Research, 67(9), pp.1310-1324.

[6] EN 1993-1-5:2006+A2:2019. Eurocode 3: Design of steel structures – Part 1–5: Plated structural elements. Brussels: European Committee for Standardization (CEN); 2019.

[7] Shokouhian, M. and Shi, Y., 2014. Investigation of ductility in hybrid and high strength steel beams. International Journal of Steel Structures, 14(2), pp.265-279.

[8] Shokouhian, M. and Shi, Y., 2015. Flexural strength of hybrid steel I-beams based on slenderness. Engineering Structures, 93, pp.114-128.

[9] Bartsch, H., Pauli, G., Eyben, F., Schaffrath, S. and Feldmann, M., 2021. Experimental and numerical investigations on the rotation capacity of high strength steel beams. ce/papers, 4(2-4), pp.1630-1636.

[10] Gittens R., Harwood K., Gedge G. (2012). Stainless Steel Composite Bridge Study-Life Cycle Cost for Maintenance Study. Arup report to Outokumpu.

[11] Kere K.J., Huang Q. (2019). Life-Cycle Cost Comparison of Corrosion Management Strategies for Steel Bridges. J. Bridge Eng., 24(4): 04019007.

[12] Karabulut B., Ferraz G., Rossi B. (2021). Lifecycle cost assessment of high strength carbon and stainless steel girder bridges. Journal of Environmental Management 277 (2021) 111460.

[13] Saliba, N. and Gardner, L., 2013. Cross-section stability of lean duplex stainless steel welded I-sections. Journal of Constructional Steel Research, 80, pp.1-14.

[14] Gardner, L., Bu, Y. and Theofanous, M., 2016. Laser-welded stainless steel I-sections: Residual stress measurements and column buckling tests. Engineering Structures, 127, pp.536-548.

[15] Bu, Y. and Gardner, L., 2018. Local stability of laser-welded stainless steel I-sections in bending. Journal of Constructional Steel Research, 148, pp.49-64.

[16] Yuan, H.X., Wang, Y.Q., Shi, Y.J. and Gardner, L., 2014. Stub column tests on stainless steel built-up sections. Thin-walled structures, 83, pp.103-114.

[17] Lalthazuala, R. and Singh, K.D., 2019. Investigations on structural performance of hybrid stainless steel I-beams based on slenderness. Thin-Walled Structures, 137, pp.197-212.

[18] Lalthazuala, R. and Singh, K.D., 2019. Structural performance of hybrid stainless steel plate girders under shear. Thin-Walled Structures, 143, p.106214.

[19] Lalthazuala, R. and Singh, K.D., 2020, October. Structural behaviour of hybrid stainless steel stub columns under axial compression. In Structures (Vol. 27, pp. 128-140). Elsevier.

[20] EN 1993-1-4:2006+A2:2020. Eurocode 3. Design of steel structures. General rules. Supplementary rules for stainless steels. Brussels: European Committee for Standardization (CEN); 2020.

[21] Gardner, L., 2008. The continuous strength method. Proceedings of the Institution of Civil Engineers-Structures and Buildings, 161, pp.127-33.

[22] ABAQUS/standard user's manual. Version 6.17. Dassault Systemes Simulia Corp.

[23] EN 1993-1-1:2005+A1:2014. Eurocode 3: Design of steel structures – Part 1–1: General rules and rules for building. Brussels: European Committee for Standardization (CEN); 2014.

[24] Rasmussen, K.J., 2003. Full-range stress–strain curves for stainless steel alloys. Journal of constructional steel research, 59(1), pp.47-61.

[25] Mirambell, E. and Real, E., 2000. On the calculation of deflections in structural stainless steel beams: an experimental and numerical investigation. Journal of Constructional Steel Research, 54(1), pp.109-133.

[26] Quach, W.M., Teng, J.G. and Chung, K.F., 2008. Three-stage full-range stress-strain model for stainless steels. Journal of Structural Engineering, 134(9), pp.1518-1527.

[27] Hradil, P., Talja, A., Real, E., Mirambell, E. and Rossi, B., 2013. Generalized multistage mechanical model for nonlinear metallic materials. Thin-walled structures, 63, pp.63-69.

[28] Bock, M., Gardner, L. and Real, E., 2015. Material and local buckling response of ferritic stainless steel sections. Thin-Walled Structures, 89, pp.131-141.

[29] Theofanous, M. and Gardner, L., 2009. Testing and numerical modelling of lean duplex stainless steel hollow section columns. Engineering Structures, 31(12), pp.3047-3058.

[30] Theofanous, M. and Gardner, L., 2010. Experimental and numerical studies of lean duplex stainless steel beams. Journal of Constructional Steel Research, 66(6), pp.816-825.

[31] Theofanous, M., Chan, T.M. and Gardner, L., 2009. Flexural behaviour of stainless steel oval hollow sections. Thin-Walled Structures, 47(6-7), pp.776-787.

[32] Theofanous, M., Chan, T.M. and Gardner, L., 2009. Structural response of stainless steel oval hollow section compression members. Engineering structures, 31(4), pp.922-934.

[33] Theofanous, M., Saliba, N., Zhao, O. and Gardner, L., 2014. Ultimate response of stainless steel continuous beams. Thin-Walled Structures, 83, pp.115-127.

[34] Gkantou, M., Kokosis, G., Theofanous, M. and Dirar, S., 2019. Plastic design of stainless steel continuous beams. Journal of Constructional Steel Research, 152, pp.68-80.

[35] Gkantou, M., Bock, M. and Theofanous, M., 2021. Design of stainless steel cross-sections with outstand elements under stress gradients. Journal of Constructional Steel Research, 179, p.106491.

[36] Chacón, R., Mirambell, E. and Real, E., 2009. Influence of designer-assumed initial conditions on the numerical modelling of steel plate girders subjected to patch loading. Thin-walled structures, 47(4), pp.391-402.

[37] Chacón, R., Mirambell, E. and Real, E., 2010. Hybrid steel plate girders subjected to patch loading, Part 1: Numerical study. Journal of Constructional Steel Research, 66(5), pp.695-708.

[38] Rasmussen, K.J.R. and Hancock, G.J., 1993. Design of cold-formed stainless steel tubular members II: Beams. Journal of Structural Engineering (ASCE) 1993;119:2368-86.

[39] Jandera, M., Gardner, L. and Machacek, J., 2008. Residual stresses in cold-rolled stainless steel hollow sections. Journal of Constructional Steel Research, 64(11), pp.1255-1263.

[40] Gardner, L. and Cruise, R.B., 2009. Modeling of residual stresses in structural stainless steel sections. Journal of Structural Engineering, 135(1), pp.42-53.

[41] Cruise, R.B. and Gardner, L., 2008. Residual stress analysis of structural stainless steel sections. Journal of constructional steel research, 64(3), pp.352-366.

[42] Dawson, R.G. and Walker, A.C., 1972. Post-buckling of geometrically imperfect plates. Journal of the Structural Division, 98(1), pp.75-94.

[43] Gardner, L. and Nethercot, D.A., 2004, October. Numerical modeling of stainless steel structural components-a consistent approach. American Society of Civil Engineers.

[44] EN 1993-1-2:2005+A1:2014. Eurocode 3: Design of steel structures – Part 1–2: General rules – Structural fire design. Brussels: European Committee for Standardization (CEN); 2014.

[45] Baddoo, N. R., 2017. SCI Publication P413: Design manual for structural stainless steel. 4th Edition. The Steel Construction Institute, UK.

[46] Gardner, L. and Theofanous, M., 2008. Discrete and continuous treatment of local buckling in stainless steel elements. Journal of Constructional Steel Research, 64(11), pp.1207-1216.

[47] Afshan, S. and Gardner, L., 2013. The Continuous Strength Method for structural stainless steel design. Thin-Walled Structures, 68, pp.42-49.

[48] Zhao, O., Afshan, S., & Gardner, L., 2017. Structural response and continuous strength method design of slender stainless steel cross-sections. Engineering Structures, 140, pp.14-25

[49] Schafer, B., 1997. CUFSM-Cross-section elastic buckling analysis v 5.04. Thin-walled Structures Group, Civil and Systems Engineering, Johns Hopkins University.